1993

A Magnetic Suspension System With a Large Angular Range

Colin P. Britcher
Old Dominion University, cbritche@odu.edu

Mehran Ghofrani
Old Dominion University

Original Publication Citation

Britcher, C. P., & Ghofrani, M. (1993). A magnetic suspension system with a large angular range. *Review of Scientific Instruments, 64*(7), 1910-1917. doi:10.1063/1.1143976

A magnetic suspension system with a large angular range

Colin P. Britcher and Mehran Ghofrani
Department of Mechanical Engineering and Mechanics, Old Dominion University, Norfolk, Virginia 23529-0247

(Received 12 February 1993; accepted for publication 7 April 1993)

In order to explore and develop technology required for the magnetic suspension of objects over large ranges of orientation, a small-scale laboratory system, the large-angle magnetic suspension test fixture (LAMSTF) has been constructed at NASA Langley Research Center. This apparatus falls into the category of large-gap, actively stabilized magnetic levitation systems. The hardware comprises five conventional electromagnets in a circular arrangement, each driven from a separate bipolar power amplifier. Electromagnet currents are commanded by a digital control system, implemented on a microcomputer, which in turn derives the position and attitude of the suspended element from an infrared optical system. The suspended element is a cylindrical, axially magnetized, permanent magnet core, within an aluminum tube. The element is "levitated" by repulsive forces, with its axis horizontal, 0.1 m above the top plane of the electromagnet conductor. The element is stabilized in five degrees-of-freedom, with rotation about the cylinder axis not controlled. By mechanical rotation of the sensor assembly, the suspended element can be made to undergo a full 360° rotation about the vertical axis. The controller accommodates the changes in magnetic coupling between the electromagnets and the suspended element by real-time adaptation of a decoupling matrix. This report presents a review of the background to the problem of magnetic suspension over large ranges of orientation. Next, the design and operation procedures adopted for LAMSTF, and the system hardware are described. Finally, some performance measurements are shown, together with illustration that the major design objective—the 360° rotation, has been accomplished.

I. INTRODUCTION

A magnetic suspension system stabilized by a feedback controller was demonstrated in 1937 by Holmes and Beams at the University of Virginia.[1,2] Since then, such devices have seen a wide range of applications in a number of areas, notably magnetic bearings, vibration isolation systems, Maglev trains, and the suspension of aerodynamic models in wind tunnels. For a broad perspective of recent developments and applications the reader is encouraged to consult Refs. 3–6. During many years of research, a great variety of design aspects have been addressed, including electromagnet configurations, position and other sensors, power amplifiers, and control systems. More recently there has been particular interest in the design and implementation of digital controllers for magnetic suspensions.[7–9] Some new applications related to future space missions are now being examined, such as payload manipulation, large angular range pointing mounts, and microgravity vibration isolation. These new applications require additional research and development in specific areas, one of which addressed in this article.

In most current magnetic suspension applications, the basic magnetic configuration is fixed. That is to say, either relatively small motion of the suspended object relative to the suspension electromagnets is allowed or the configuration is chosen such that large motions do not cause variation in the magnetic circuit geometry. Examples of the latter are rotation about the spin axis in a magnetic bearing or motion along the track in Maglev. This configuration invariance generally leads to feedback controllers being designed with fixed parameters, most importantly gains. An exception worthy of note is the practice of deliberately changing controller gains in certain applications involving flexible rotors supported by magnetic bearings, when the rotor approaches a critical speed.

In some cases, however, it is desirable to permit larger and more general angular motions of the suspended object. An interesting example is wind tunnel model magnetic suspension and balance systems (MSBSs), where aerodynamic tests might be carried out over a large range of angles-of-attack. Large changes in orientation of the suspended object generally cause large changes in the magnetic coupling between electromagnets and the suspended object, such that a fixed parameter controller which can maintain stability over the full desirable range cannot be devised. Slightly improved performance could be achieved by varying the gains in each control loop as a function of orientation. This corresponds to the "gain scheduling" approach, well-known in other applications. Here, however, the coupling variations are so strong that something more is required. An obvious approach, and the one being pursued in this article, is to counteract the variations of coupling between the suspension electromagnets and the suspended object by incorporating a variable "decoupling" stage in the control loop, as illustrated in Fig. 1. In practice, this variable stage takes the form of a matrix with variable elements inserted into the latter stages of a digital controller.

 0034-6748/93/64(7)/1910/8/$6.00

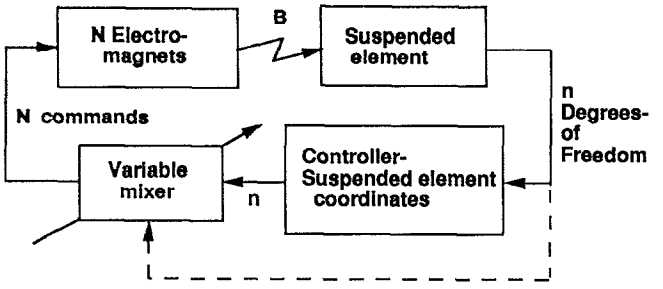

FIG. 1. Conceptual controller layout with variable decoupling stage.

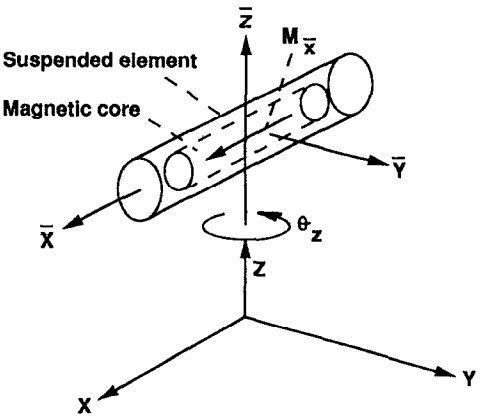

FIG. 2. General configuration—axis systems and nomenclature.

II. EARLY WORK

Pioneering work was carried out at the University of Southampton in relation to the wind tunnel MSBS problem. It was decided to study the extension of the angle-of-attack range of the Southampton MSBS, with the goal of a 90° range. The thinking was that a series of fixed parameter controllers could be designed with appropriate decoupling matrices calculated for a number of different angles-of-attack of the suspended wind tunnel model. If each controller was reasonably robust, then it could provide stable suspension over a significant range of angle-of-attack. As the limit of the usable range of each controller was approached, the controller parameters would be somehow switched to cover a new range of attitudes. Using this approach, a range of angle-of-attack of 0°–60° was achieved with a "two-point" controller, designed for 15° and 45° angle-of-attack as early as 1982.[10] Major refinements were made in later work and suspension over a range of angle-of-attack from $-6°$ to $+96°$ was achieved in 1988[11,12] with controller parameters calculated every 1°. This range was limited by the position sensing system, which was a conceptually simple, though mechanically quite elaborate, optical system,[11] not by control or other difficulties.

Some other work is also worthy of note. A laboratory prototype of an advanced technology Control Moment Gyro (CMG) was demonstrated by SatCon Technology Corporation in 1990.[13] This device consists of a persistant-mode superconducting solenoid magnetically suspended within a spherical assembly of support coils and capable of being slewed through large angles. The symmetry of the supporting coils is such that this can be achieved with a variable decoupling stage that resembles a straightforward coordinate transformation.

In order to further refine design and control techniques for the magnetic suspension of objects over large angular ranges, a laboratory-scale demonstration apparatus, the large-angle magnetic suspension test fixture (LAMSTF), was constructed at NASA Langley Research Center (LaRC), starting in late 1989, and will be the main focus of this article.

III. TECHNICAL BACKGROUND

Following traditional practice,[14] the magnetic forces and moments acting on a magnetized core in an applied magnetic field can be written as follows:

$$\mathbf{F}_c=\int_V \mathbf{M}.\nabla\mathbf{B}dV, \quad \mathbf{T}_c=\int_V \mathbf{M}\times\mathbf{B}dV, \tag{1}$$

where $\mathbf{M}$ represents the magnetization of the magnetic core in A/m, $\mathbf{B}$ the applied flux density in T, and V the volume of the core in m^3. In many cases, most particularly where a permanent magnet core is employed, the magnetization can be assumed constant over the core volume. In applications involving large air gaps, it is also frequently possible to regard the applied magnetic field gradients as relatively uniform over the core, such that

$$\mathbf{F}_c\simeq V(\mathbf{M}.\nabla\mathbf{B}_o), \quad \mathbf{T}_c\simeq V(\mathbf{M}\times\mathbf{B}_o), \tag{2}$$

where the subscript o indicates that the field or field gradient is evaluated at the centroid of the magnetic core. Now, following the detailed development presented in Ref. 15, the effect of changes in relative orientation between the magnetic core and the electromagnet array can be incorporated as follows:

$$\bar{\mathbf{F}}_c=V[T_m][\partial B][T_m]^{-1}\bar{\mathbf{M}}, \tag{3}$$

$$\bar{\mathbf{T}}_c=V\bar{\mathbf{M}}\times([T_m]\mathbf{B}), \tag{4}$$

where a bar over a variable indicates magnetic core coordinates, $[\partial B]$ is a matrix of field gradients, and $[T_m]$ is the coordinate transformation matrix from electromagnet coordinates to suspended element (magnetic core) coordinates. The axis systems and some nomenclature is clarified in Fig. 2.

The fields and field gradients are created by an array of N electromagnets. Thus we can write

$$\mathbf{B}=[K_B]\frac{\mathbf{I}}{I_{\max}}, \tag{5}$$

where $\mathbf{I}=(I_1,I_2,...,I_N)^T$ and $[K_B]$ represents a matrix of field coefficients. Similarly, each element of $[\partial B]$ can be written

$$\partial B_{ij}=[K_{\partial B_{ij}}]\frac{\mathbf{I}}{I_{\max}}. \tag{6}$$

At this stage, the equations are quite general, but will now be considerably simplified for the LAMSTF application to be described later. First, the magnetization of the suspended element is assumed to be along its principal ($\bar{x}$) axis

$$\bar{\mathbf{M}}=(M_{\bar{x}},0,0). \tag{7}$$

Continuing, the only large rotation of the suspended element is assumed to take place about the z axis, so $[T_m]$ becomes

$$[T_m]=\begin{bmatrix}\cos\theta_z & \sin\theta_z & 0\\ -\sin\theta_z & \cos\theta_z & 0\\ 0 & 0 & 1\end{bmatrix} \tag{8}$$

Substituting, expanding and collecting terms:

$$\begin{bmatrix}T_{\bar{y}}\\ T_{\bar{z}}\\ F_{\bar{x}}\\ F_{\bar{y}}\\ F_{\bar{z}}\end{bmatrix}=\begin{bmatrix}[KT]\\ [KF]\end{bmatrix}\mathbf{I}, \tag{9}$$

where

$$[KT]=\begin{bmatrix}-[K_z]\\ -\sin\theta_z[K_x]+\cos\theta_z[K_y]\end{bmatrix}, \tag{10}$$

$$[KF]=\begin{bmatrix}\cos^2\theta_z[K_{xx}]+2\cos\theta_z\sin\theta_z[K_{xy}]+\sin^2\theta_z[K_{yy}]\\ -\cos\theta_z\sin\theta_z[K_{xx}]+(\cos^2\theta_z-\sin^2\theta_z)[K_{xy}]+\cos\theta_z\sin\theta_z[K_{yy}]\\ \cos\theta_z[K_{xz}]+\sin\theta_z[K_{yz}]\end{bmatrix}. \tag{11}$$

Now there are two related problems to solve. First, the equilibrium currents required to support the weight of the suspended element may be found by using

$$\begin{aligned}&F_z=F_{\bar{z}}=m_c g=VM_{\bar{x}}B_{\bar{x}\bar{z}},\\ &T_{\bar{y}}=T_{\bar{z}}=F_{\bar{x}}=F_{\bar{y}}=0,\end{aligned} \tag{12}$$

where m_c is the mass of the suspended element. Equation (9) can now be solved for required currents as a function of yaw orientation θ_z. As a point of interest

$$B_{\bar{x}\bar{z}}=\frac{m_c g}{VM_{\bar{x}}}=0.0962\ \text{T/m in this case.} \tag{13}$$

Second, the decoupling matrix can be found by direct inversion of the $[KT/KF]$ matrix from Eq. (9), giving

$$\mathbf{I}_{\text{demand}}=\begin{bmatrix}[KT]\\ [KF]\end{bmatrix}^{-1}\begin{bmatrix}T_{\bar{y}}\\ T_{\bar{z}}\\ F_{\bar{x}}\\ F_{\bar{y}}\\ F_{\bar{z}}\end{bmatrix}_{\text{demand}} \tag{14}$$

Note that the $[KT/KF]$ matrix is a function of θ_z. In practice, it has been found convenient to normalize the inverted $[KT/KF]$ matrix column-by-column, with the normalization factor being incorporated into the loop gain.

IV. THE LARGE-ANGLE MAGNETIC SUSPENSION TEST FIXTURE

A. Configuration

The basic design objectives for the LAMSTF were to suspend a cylindrical element containing a permanent magnet core, to demonstrate stability and control of the suspended element in at least five degrees-of-freedom, and to permit controlled rotation of the suspended element in one degree-of-freedom over the full range of 360°. For various reasons, a design constraint was imposed that all suspension and control electromagnets were to be located behind a flat plane, located some distance from the suspended element. Since this was a ground-based experiment, the plane was chosen to be horizontal, with the element "lev-

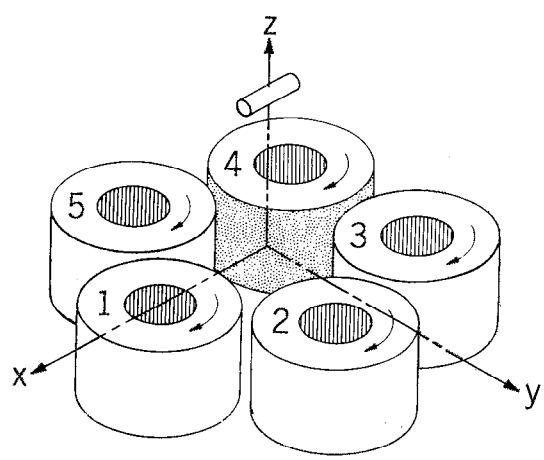

FIG. 3. Configuration of the large-angle magnetic suspension test fixture.

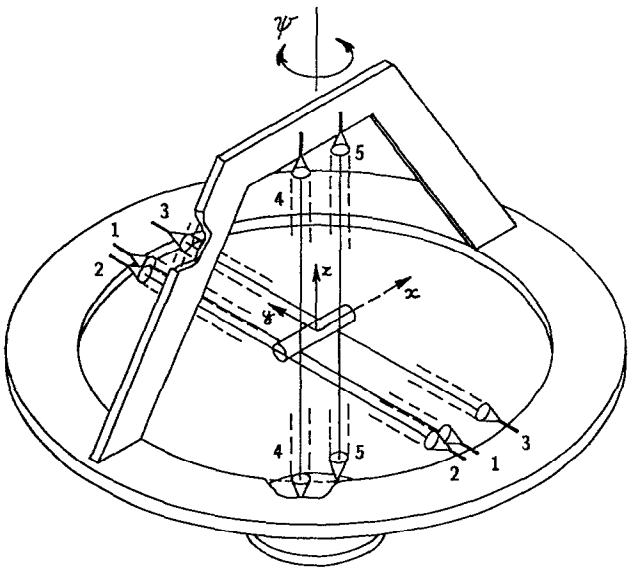

FIG. 4. Schematic diagram of the position sensor assembly.

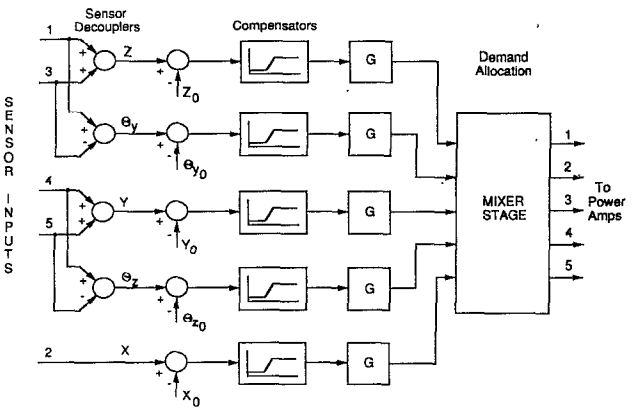

FIG. 5. Controller block diagram.

itated" above the plane by repulsive forces and with the large angular rotation performed about a vertical axis, the z (yaw) axis indicated in Fig. 3. The uncontrolled degree-of-freedom is rotation about the axis of magnetization of the magnetic core, the x(roll) axis in Fig. 3. This novel configuration represents the simplest form of a family of "planar array" configurations.[15] The fact that the suspended element is "levitated" by repulsive forces, rather than the attractive forces more usually exploited, does present certain additional difficulties. Most important, the suspended element proves to be quite strongly unstable in two degrees-of-freedom and weakly unstable in a third.[15] The strong instability arises due the presence of an axial field along the axis of magnetization, but in the negative x direction, causing a tendency for the suspended element to reverse its direction in this field—a "compass needle" effect.

B. Hardware description

The general configuration was illustrated earlier in Fig. 3. An array of five, room-temperature, copper electromagnets are equally spaced on a 13.77 cm radius. The coils are wound with 509 turns of AWG 10 enamelled copper wire on bakelite forms, with mild steel cores. There is no provision for active cooling, since the operation of LAMSTF tends to be rather intermittent in nature. The design maximum steady-state current is around 15 A, limited by the rate of temperature rise. Thermocouples are embedded in the windings, connected to over-temperature alarms and power cutouts. The electromagnets are mounted on a heavy aluminum plate 1.27 cm thick. Each electromagnet is driven by a transistor switching power amplifier, rated at ± 150 V and ± 30 A continuous, with the capability of full four-quadrant operation. The switching frequency is 22 kHz.

The suspended element consists of 16 wafers of neodymium–iron–boron permanent magnet material, each approximately 0.8 cm in diameter and 0.3175 cm thick, epoxied into an aluminum tube, 5.32 cm long and 0.9525 cm o.d. The total mass of the suspended element is 22.5 g and the moment of inertia about tranverse axes is 5.5×10^{-6} kg m^2. The direction of magnetization is along the axis of the cylinder, which is horizontal when suspended. The nominal magnetization is 954 930 A/m (1.2 T), although measurements have indicated a slightly lower working value. The suspension height is 0.1 m, measured from the axis of the suspended element to the top plane of the electromagnet conductor.

The position sensing system follows a traditional approach of multiple light beams partially interrupted by the suspended element. In this case, the beams are arranged in the vertical and horizontal planes. The light sources are miniature infrared light-emitting diodes, intended for use with fiber optics, with collimating lenses added. The light receivers are matching infrared phototransistors, with focusing lenses added. The complete sensor system is mounted on a framework which can be rotated by hand about a vertical axis. A schematic diagram of the position sensor assembly is shown in Fig. 4.

C. Controllers

To facilitate the earliest commissioning of LAMSTF, a simple analog controller was constructed, following traditional practices for large-gap magnetic suspension systems. In the controller, position sensor outputs are summed and differenced, where appropriate, to derive displacement signals in suspended element axes, that is, axial, lateral, and vertical translations (x,y,z) and pitch and yaw rotations (θ_y,θ_z). Each signal is processed independently by dual

phase-advance ("lead") compensators connected in series, with a variable overall gain. The required decoupling matrix is implemented as a mixer stage at the output of the compensators. A block diagram of the controller is shown in Fig. 5. Since variation of the decoupling coefficients as a function of yaw orientation is a practical impossibility with an analog controller, this controller was only used to suspend at a single, fixed yaw orientation [$\theta_z=0$ in Eqs. (9)–(11)].

A first-generation digital controller was generated as a digital simulation of the analog controller, using a bilinear (Tustin's) transformation.[16] The control algorithm is implemented on a 386-class PC, coded in C. Data input and output is handled by standard 12-bit A/D and D/A boards, respectively. The controller sample interval and time delay are approximately equal and are typically set at 2.5 ms, controlled by an internal or external clock. Suspended element position and attitude can be displayed in real time on an oscilloscope-like screen display. Controller parameters, such as loop gains, can be changed in real time from the keyboard. Variable size steps can be commanded in each degree-of-freedom, with automatic recording of data to disk for future processing.

V. MATHEMATICAL MODELS

Classical controller design procedures typically require a linear mathematical model of the plant that is to be controlled. The LAMSTF plant is nonlinear due the large angular excursions required, but can be linearized about any chosen operating point in the usual way. The following state-space model results:[15]

$$\{\dot{\delta X}\}=\mathbf{A}\{\delta X\}+\mathbf{B}\{\delta I\}$$

where

$$\{\delta X\}^T=\{\Omega_{\bar{y}}\,\Omega_{\bar{z}}\,\theta_y\,\theta_z\,\mathrm{V}_{\bar{x}}\,\mathrm{V}_{\bar{y}}\,\mathrm{V}_{\bar{z}}\,x\,y\,z\};$$

Ω represents angular velocities, V represents linear velocities, and

$$\mathbf{A}=\mathscr{W}\begin{bmatrix}
0 & 0 & -B_x & 0 & 0 & 0 & 0 & -B_{xz} & -B_{yz} & -B_{zz}\\
0 & 0 & 0 & -B_x & 0 & 0 & 0 & B_{xy} & B_{yy} & B_{yz}\\
1 & 0 & 0 & 0 & 0 & 0 & 0 & 0 & 0 & 0\\
0 & 1 & 0 & 0 & 0 & 0 & 0 & 0 & 0 & 0\\
0 & 0 & -B_{xz} & 2B_{xy} & 0 & 0 & 0 & (B_{xx})_x & (B_{xx})_y & (B_{xx})_z\\
0 & 0 & B_{yz} & (B_{yy}-B_{xx}) & 0 & 0 & 0 & (B_{xy})_x & (B_{xy})_y & (B_{xy})_z\\
0 & 0 & (B_{xx}-B_{zz}) & B_{yz} & 0 & 0 & 0 & (B_{xz})_x & (B_{xz})_y & (B_{xz})_z\\
0 & 0 & 0 & 0 & 1 & 0 & 0 & 0 & 0 & 0\\
0 & 0 & 0 & 0 & 0 & 1 & 0 & 0 & 0 & 0\\
0 & 0 & 0 & 0 & 0 & 0 & 1 & 0 & 0 & 0
\end{bmatrix},$$

$$\mathscr{W}=VM_{\bar{x}}\begin{bmatrix}
\frac{1}{I_c} & & & & & & & & & \\
 & \frac{1}{I_c} & & & & & & & & \\
 & & 1 & & & & \cdots & 0 & \cdots & \\
 & & & 1 & & & & & & \\
 & & & & \frac{1}{m_c} & & & & & \\
 & & & & & \frac{1}{m_c} & & & & \\
 & & & & & & \frac{1}{m_c} & & & \\
 & & \cdots & 0 & \cdots & & & 1 & & \\
 & & & & & & & & 1 & \\
 & & & & & & & & & 1
\end{bmatrix},$$

$$\mathbf{B}=\frac{1}{I_{\max}}\mathscr{W}\begin{bmatrix} -K_{z_1} & -K_{z_2} & -K_{z_3} & -K_{z_4} & -K_{z_5} \\ K_{y_1} & K_{y_2} & K_{y_3} & K_{y_4} & K_{y_5} \\ & & \cdots 0 \cdots & & \\ & & \cdots 0 \cdots & & \\ K_{xx_1} & K_{xx_2} & K_{xx_3} & K_{xx_4} & K_{xx_5} \\ K_{xy_1} & K_{xy_2} & K_{xy_3} & K_{xy_4} & K_{xy_5} \\ K_{xz_1} & K_{xz_2} & K_{xz_3} & K_{xz_4} & K_{xz_5} \\ & & \cdots 0 \cdots & & \\ & & \cdots 0 \cdots & & \\ & & \cdots 0 \cdots & & \end{bmatrix}.$$

I_c is the transverse moment of inertia of the (cylindrical) suspended element. An important point to note is that the **A** matrix is composed of equilibrium field, field gradient, and "second-order gradient" (gradient of gradient) terms. Numerical values can be found in Ref. 17.

The eigenvalues of this matrix give the natural behavior of the plant and are found, in the case of LAMSTF, to be

Mode No.	Eigenvalue	Characterics and mode shape
Mode 1	59.26 rad/s	Unstable divergence; Pitch rotation and axial translation
Mode 2	7.972	Stable oscillation; Axial translation and pitch rotation
Mode 3	58.294	Unstable divergence; Yaw rotation
Mode 4	0.956	Stable oscillation; Vertical translation
Mode 5	9.776	Unstable divergence; Lateral translation

Modes 1 and 3 are referred to as the "compass needle" modes, since they arise from the tendency of the suspended element to reverse its direction in the applied axial field, $B_{\bar{x}}$. They are the most important from the control point of view, since they have the highest unstable natural frequencies, close to 10 Hz here.

In addition, linear models have been developed for the coil/power supply assembly, including mutual inductances, some eddy-current effects and, of course, the controller.

VI. RESULTS

The analog controller, even with rather crudely estimated parameters, achieved successful suspension. Manual trimming of gains permitted reasonable damping to be achieved in all degrees-of-freedom. As soon as the remainder of the LAMSTF hardware was properly checked out, the analog controller was replaced by the first-generation digital version, which is functionally similar. Again, suspension was relatively easy to achieve, with a little manual fine tuning.

The measured damping in four degrees-of-freedom (three translations and yaw rotation) is typically slightly less than that predicted by using the linear simulation, with equivalent loop gains, as shown in Fig. 6. This is presumed to be due to an inaccurate estimation of certain parameters

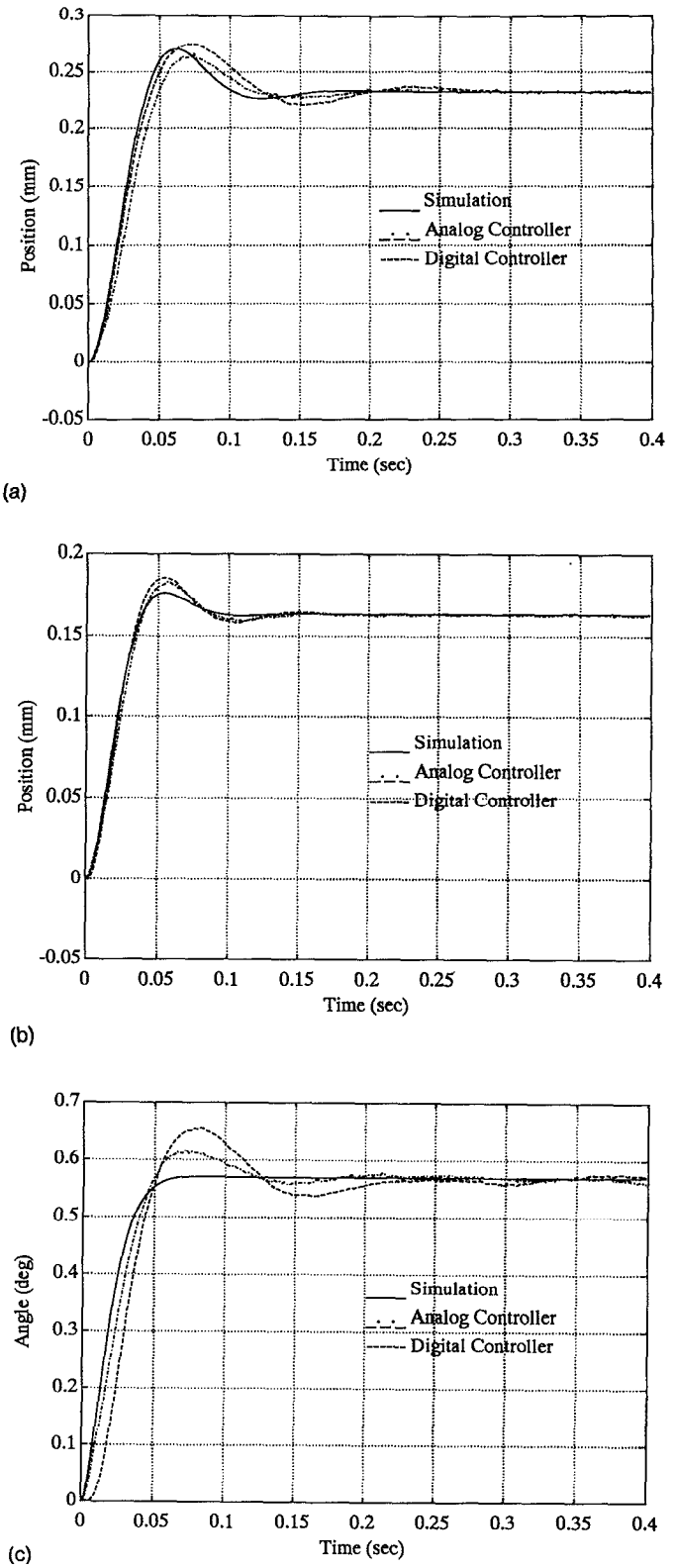

FIG. 6. Simulated and actual step responses (y translation and yaw rotation similar).

and the omission of minor dynamic effects. One degree-of-freedom, rotation in pitch, shows substantially lower damping than predicted. This has yet to be satisfactorily explained, although it is presently thought most likely due to some form of eddy current effect. It should be noted that pitch rotation is initiated by a change in vertical field

through the entire LAMSTF assembly, whereas all other degrees-of-freedom require no change in total flux through the assembly.

With the digital controller, the 360° yaw rotation was easily accomplished. The variable decoupling matrix was added just prior to the D/A output routines. A set of 60 mixing matrices were calculated from Eq. (14), at 6° intervals (the fivefold symmetry about the vertical axis is helpful here). The controller interpolates in real time between these matrices. The first three matrices, individually normalized, are shown here for reference:

$$\mathbf{I}_{\text{demand}_{\theta=0^\circ}}=\begin{bmatrix} 0.7713 & 0 & 1 & 0 & -1 \\ 1 & 1 & -0.8091 & 0.6182 & -0.3092 \\ 0.8584 & 0.6178 & 0.3091 & -1 & 0.8092 \\ 0.8584 & -0.6178 & 0.3091 & 1 & 0.8092 \\ 1 & -1 & -0.8091 & -0.6182 & -0.3092 \end{bmatrix}\begin{bmatrix} T_{\bar{y}} \\ T_{\bar{z}} \\ F_{\bar{x}} \\ F_{\bar{y}} \\ F_{\bar{z}} \end{bmatrix}_{\text{demand}},$$

$$\mathbf{I}_{\text{demand}_{\theta=6^\circ}}=\begin{bmatrix} 0.7637 & -0.1069 & 1 & -0.2091 & -1 \\ 0.9695 & 0.9340 & -0.6841 & 0.7474 & -0.409 \\ 0.8728 & 0.6841 & 0.1068 & -1 & 0.7472 \\ 0.8234 & -0.5112 & 0.5112 & 0.8708 & 0.8708 \\ 1 & -1 & -0.9339 & -0.4091 & -0.209 \end{bmatrix}\begin{bmatrix} T_{\bar{y}} \\ T_{\bar{z}} \\ F_{\bar{x}} \\ F_{\bar{y}} \\ F_{\bar{z}} \end{bmatrix}_{\text{demand}},$$

$$\mathbf{I}_{\text{demand}_{\theta=12^\circ}}=\begin{bmatrix} 0.7655 & -0.2091 & 0.9339 & -0.409 & -1 \\ 0.9405 & 0.8708 & -0.5111 & 0.8708 & -0.5112 \\ 0.8916 & 0.7472 & -0.1068 & -1 & 0.6841 \\ 0.7958 & -0.409 & 0.6840 & 0.7472 & 0.9339 \\ 1 & -1 & -1 & -0.209 & -0.1069 \end{bmatrix}\begin{bmatrix} T_{\bar{y}} \\ T_{\bar{z}} \\ F_{\bar{x}} \\ F_{\bar{y}} \\ F_{\bar{z}} \end{bmatrix}_{\text{demand}}.$$

To permit this interpolation, the controller must have information as to the actual yaw orientation of the suspended element. It was realized that under certain circumstances this information could be deduced in near real time from the observed behavior of the suspended element, in at least two ways.

A. Yaw error tracking

Suspension is established at a known reference orientation. If the sensor framework is now rotated (by hand) through some small angle, the suspended element will tend to become misaligned relative to the sensors. This yaw error signal is filtered to remove the effects of noise and the natural motion of the suspended element in response to small disturbances. Once the filtered error reaches a preset threshold, the controller steps through the decoupling matrix array, in an attempt to drive the yaw error back to zero. This method is rather crude, but has proven to be unexpectedly reliable.

B. Current distribution analysis

The predicted current distributions required to suspend at various yaw orientations, together with actual measurements, are shown in Fig. 7. It should be noted that the distributions are almost perfectly sinusoidal in nature. By straightforward analysis of an observed current distribution, again with some filtering to remove the effects of noise and so forth, it is possible to deduce the orientation of the suspended element.

In both cases, the algorithm cannot accommodate a steady-state applied yaw torque. Nevertheless, the fact that the position sensor framework does not require any form of

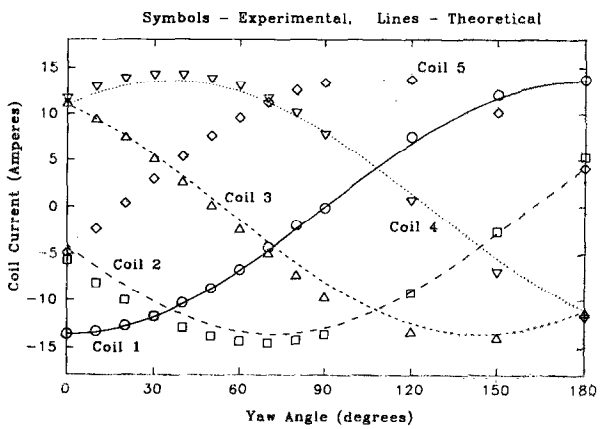

FIG. 7. Predicted and measured equilibrium suspension currents.

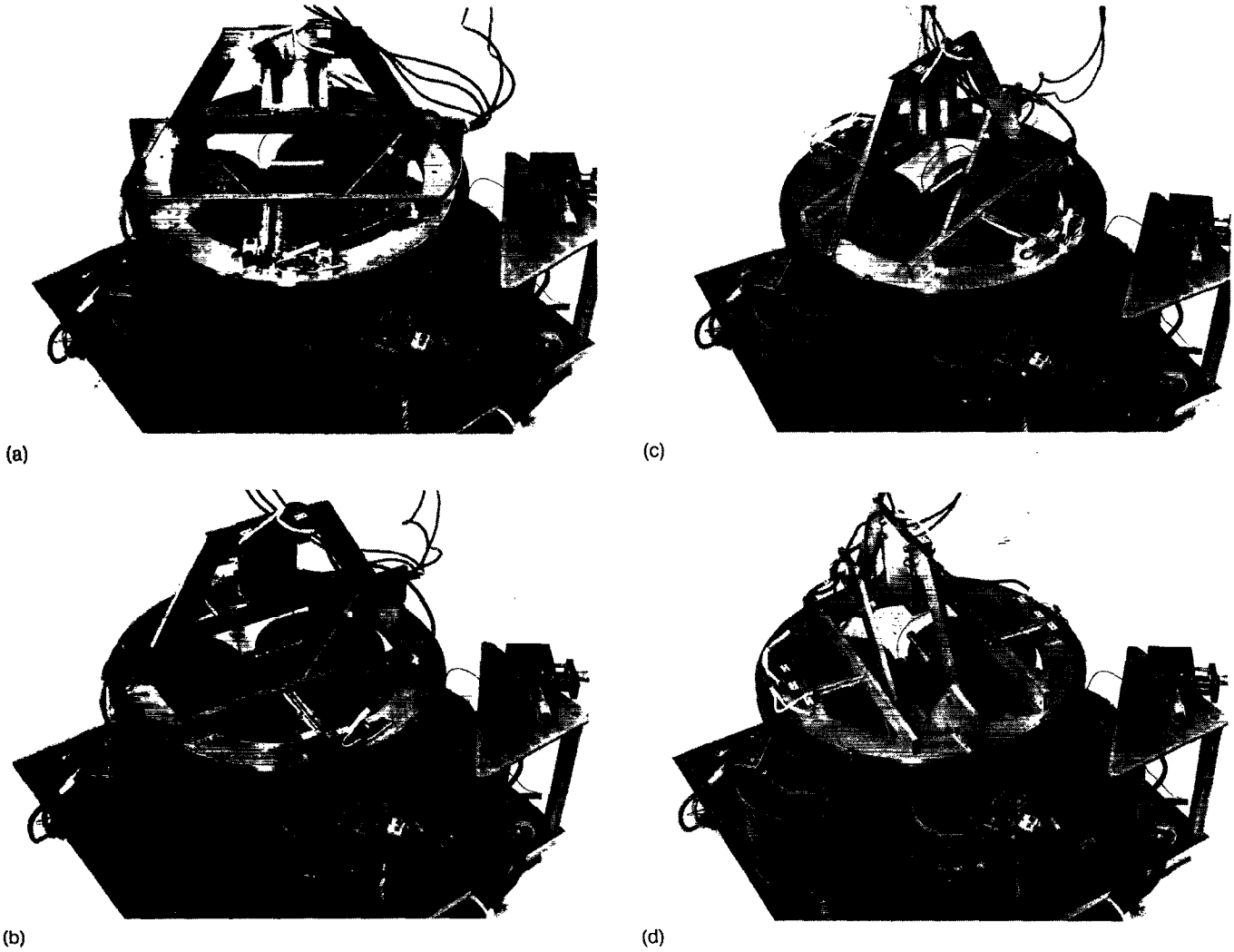

FIG. 8. Large angular excursions in yaw (a) 0 deg (datum orientation); (b) 30 deg; (c) 60 deg; (d) 120 deg.

angular orientation sensor is a great practical advantage. A sequence of photographs showing the system in operation is shown as Fig. 8.

ACKNOWLEDGMENTS

This work was supported by NASA Langley Research Center under Grant NAG-1-1056. The Technical Monitor was Nelson J. Groom of the Spacecraft Controls Branch. In addition, the authors wish to acknowledge the assistance of Thomas C. Britton of Lockheed Engineering and Sciences Company.

[1] F. T. Holmes, Rev. Sci. Instrum. **8**, 444 (1937).
[2] F. T. Holmes, J. W. Beams, Nature **140**, 30 (1937).
[3] B. V. Jayawant, Proc. R. Soc. London A **416**, 245 (1988).
[4] N. J. Groom, ed., NASA CP-3152, Pts.I&II (1992).
[5] P. E. Allaire, ed., 3rd Int. Symp. Mag. Bearings, Technomic (1992).
[6] J. F. Lubomski, ed., NASA CP-10094, (1991).
[7] A. T. Carmichael, S. Hinchliffe, P. N. Murgatroyd, and I. D. Williams, Rev. Sci. Instrum. **57**, 1611 (1986).
[8] M. B. Scudiere, R. A. Williams, and G. T. Gillies, Rev. Sci. Instrum. **57**, 1616 (1986).
[9] M. A. Lawson and G. T. Gillies, Rev. Sci. Instrum. **60**, 456 (1989).
[10] C. P. Britcher, NASA CR-172154 (1982).
[11] D. H. Parker, NASA CR-181895 (1989).
[12] M. J. Goodyer, NASA CP-3152, 775 (1992).
[13] J. R. Downer, D. A. Bushko, V. Gondhalekar, and R. P. Torti, NASA CP-3152, 955 (1992).
[14] T. Stephens, NASA CR-66903 (1969).
[15] N. J. Groom and C. P. Britcher, NASA TP-3229 (1992).
[16] W. A. Kilgore, NASA CR-182087 (1990).
[17] M. Ghofrani, NASA CR-191890 (1992).